# 1 550 nm long-wavelength vertical-cavity surface emitting lasers*

**LIU Li-jie (刘丽杰)[1,2], WU Yuan-da (吴远大) [1,2]**, WANG Yue (王玥)[1], AN Jun-ming (安俊明) [1,2], and HU Xiong-wei (胡雄伟)[1]**

*1. State Key Laboratory of Integrated Optoelectronics, Institute of Semiconductors, Chinese Academy of Sciences, Beijing 100083, China*

*2 College of Material Science and Optoelectronic Technology, University of Chinese Academy of Sciences, Beijing 100049, China*

(Received 14 March 2018; Revised 20 April 2018)

©Tianjin University of Technology and Springer-Verlag GmbH Germany, part of Springer Nature 2018

A 1 550 nm long-wavelength vertical cavity surface emitting laser (VCSEL) on InP substrate is designed and fabricated. The transfer matrix is used to compute reflectivity spectrum of the designed epitaxial layers. The epitaxial layers mainly consist of 40 pairs of n-$Al_xGa_yIn_{(1-x-y)}As$/InP, and 6 strain compensated $Al_xGa_yIn_{(1-x-y)}As$/InP quantum wells on n-InP substrate, respectively. The top distributed Bragg reflection (DBR) mirror system has been formed by fabricating 4.5 pairs of $SiO_2$/Si. The designed cavity mode is around 1 536 nm. The dip of the fabricated cavity mode is around 1 530 nm. The threshold current is 30 mA and the maximum output power is around 270 μW under CW operation at room temperature.

**Document code:** A **Article ID:** 1673-1905(2018)05-0342-4

**DOI** https://doi.org/10.1007/s11801-018-8037-6

Semiconductor diode lasers can be used in a variety of applications including telecommunications, displays, solid-state lighting, sensing and printing[1-4]. Among them, vertical cavity surface emitting lasers (VCSELs) are particularly promising[5]. Because VCSEL has some unique properties such as wafer-scale testing, low-cost packaging, and ease of fabrication into arrays. Low loss in optical fibers, low dispersion for 1 550 nm optical fibers, higher eye safe maximum limit power and lower operation voltage are some of the advantages of long wavelength VCSELs over 850 nm and 980 nm GaAs-based VCSELs[6,7]. Over the past decades, long-wavelength spectral regimes were reported mainly by two research teams, one of which is Chang-Hasnain team of California at Berkeley, California USA. In 2009, this group presented a high-speed VCSEL operating at date-rate up to 22 Gbit/s, and the wavelength was 1 539 nm[8]. Next year, they presented a 1 550 nm VCSEL utilizing a high contrast grating (HCG) as a top mirror and proton implantation to form an electrical aperture[9]. The other team is M.-C. Amann team of Technische Universitaet Muenchen, Garching Germany. They got a high-performance VCSEL at 1 550 nm with superior output characteristics and modulation bandwidths up to 10 Gbit/s in 2002[10]. They utilized buried tunnel junction (BTJ) and fabricated VCSEL arrays, and the data rate was up to 12.5 Gbit/s over different fiber channels[11,12]. Single-mode emission, high-speed operation, high-contrast grating devices and wavelength tuning are the international research group aim. But in China, research teams mainly focus on the wavelength range from 850 nm to 980 nm[13-16].

In this letter, we present InP-based 1 550 nm VCSELs. $Al_xGa_yIn_{(1-x-y)}As$ has been chosen as the active material[17]. A structure of VCSEL has been presented in this work, which incorporates $Al_xGa_yIn_{(1-x-y)}As$/InP bottom distributed Bragg reflection (DBR) and $SiO_2$/Si top DBR. By using a dielectric DBR, we can easily control the cavity resonance wavelength by changing the thickness of one dielectric layer, even if the initial cavity wavelength is mismatched from the gain peak or DBR center wavelength after crystal growth. Moreover, large index contrast, small penetration depth, reduced photon lifetime and larger bandwidth properties can be achieved.

For the design of high performance VCSELs, it is important to know the reflectivity spectra of the epitaxial layers in the resonator. A local minimum in the reflectivity spectrum occurs at the lasing wavelength of a longitudinal mode. We use transfer matrix method to calculate reflectivity spectrum. The transfer matrix is written as[18]

$$\boldsymbol{M}=\begin{bmatrix}\boldsymbol{B}\\ \boldsymbol{C}\end{bmatrix}=\left\{\prod_{j=1}^{N}\begin{bmatrix}\cos(kn_jd_j) & \dfrac{\mathrm{i}}{n_j}\sin(kn_jd_j)\\ \mathrm{i}n_j\sin(kn_jd_j) & \cos(kn_jd_j)\end{bmatrix}\right\}\begin{bmatrix}1\\ n_{N+1}\end{bmatrix}, \qquad (1)$$

* This work has been supported by the National High Technology and Development Program of China (No.2015AA016902).

** E-mail: wuyuanda@semi.ac.cn

$$R=\left(\frac{n_0B-C}{n_0B+C}\right)\left(\frac{n_0B-C}{n_0B+C}\right)^{*} ,\qquad (2)$$

$$\varphi=\mathrm{arctg}\left[\frac{\mathrm{i}n_0\left(CB^{*}-BC^{*}\right)}{n_0^{\ 2}\left(BB^{*}-CC^{*}\right)}\right],\qquad (3)$$

where $\boldsymbol{M}$ is a characteristic matrix, $R$ is reflectivity, $\varphi$ is reflectivity phase, $n_j$ and $d_j$ are refractive index and geometric thickness in the $j$th layer, i is imaginary unit, $k=2\pi/\lambda$, $n_0$ is incident medium refractive index, and $n_{N+1}$ is emergent medium refractive index.

According to the above three formulas, the reflectivity spectrum of the designed epitaxial layers is calculated. The epitaxial layers from bottom consist of 40 pairs of n-$Al_xGa_yIn_{(1-x-y)}As$/InP, and 6 strain compensated $Al_xGa_yIn_{(1-x-y)}As$/InP quantum wells on n-InP substrate, respectively. The top DBR mirror system has been formed by fabricating 4.5 pairs of $SiO_2$/Si. Between multiple quantum well (MQW) and DBR, the separate confinement heterojunction (SCH) structures are all fully lattice matched with the InP material. The schematic diagram of epitaxial layers is shown in Fig.1. The device is electrically injected and the proton implantation serves to form the current confining aperture. Fig.2(a) shows the simulation reflectivity spectrum. From Fig.2(b), a dip in the stop-band clearly proves the presence of a cavity mode in the resonator. The reflectivity of simulation cavity mode is around 88%. The wavelength is around 1 536 nm.

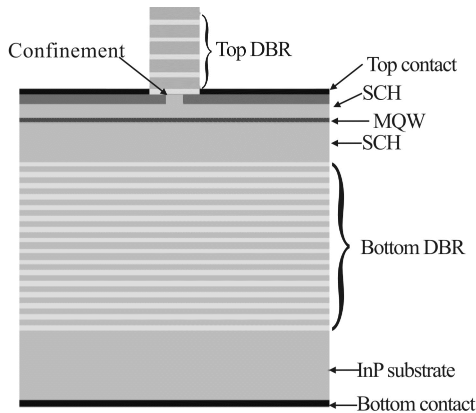


**Fig.1 Schematic diagram of VCSEL**

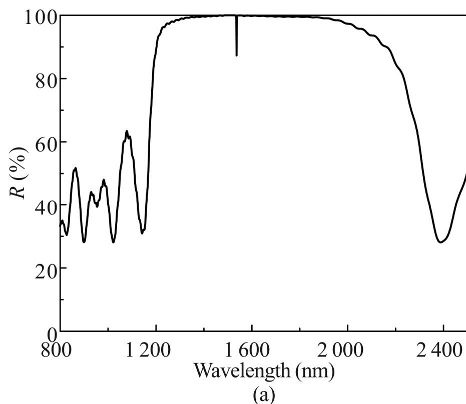


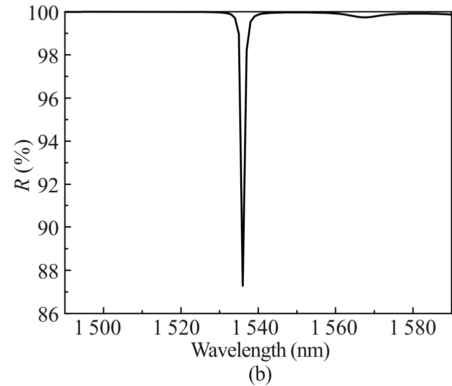


**Fig.2 (a) Epitaxial layers reflectivity spectrum of simulation diagram; (b) Cavity mode reflectivity spectrum of simulation diagram**

The devices were fabricated by InP processing platform. The bottom DBRs and active layers were grown on n-InP substrate. After the growth of the active layers and SCH, the proton was implanted by a photo-resist patterning and wet etching process to form the current confining aperture. TiPtAu top contact metals were evaporated and the light output windows were removed for dielectric top DBR mirror. A 4.5-pairs-$SiO_2$/Si dielectric DBR was evaporated by E-beam evaporation. The TiPtAu top contact metals were followed by etching of the $SiO_2$/Si layers. Finally, the NiGeAu bottom contact metals were evaporated.

Fig.3(a) is reflectivity spectrum of the all epitaxial layers structure. There is a dip in the stop-band clearly in the resonator. From Fig.3(b), the reflectivity of experiment cavity mode is around 94%. Compared with Fig.2(b), the reflectivity 94% of experiment cavity mode is lower than the simulation one 88%. There are absorption and loss from the semiconductor-dielectric interface. The maximum transmittance in the cavity mode[19] is

$$T_{\max}=\frac{T_1T_2}{\left(1-\overline{R}\right)^2} ,$$

$$\overline{R}=\sqrt{R_1R_2} ,\qquad (4)$$

where $R_1$ and $R_2$ are the reflectivities of top and bottom DBRs, respectively. $T_1$ and $T_2$ are the transmittances of top and bottom DBRs, respectively. If there is no absorption and loss in all reflectance coatings and the reflectance coating is symmetrical, we will get

$$R_1=R_2,\ T_1=T_2=1-R_1 .\qquad (5)$$

The maximum transmittance is 1. However, the interface is not ideal in the experiment process. For example, we have three lithography processes before sputtering $SiO_2$/Si DBR. There may be residue in the interface after the cleaning process or the reflectance coatings quality is not good, which can bring about absorption and loss. We can improve that by adjusting the process order so that lithography process times are decreased and keeping the interface clean in the photoresist removing process.

The cavity mode wavelength is around 1 530 nm. The

cavity mode wavelength deviates by 6nm forward shorter wavelength from 1 536 nm to 1 530 nm. This is because every layer thickness in monolithic growth is thinner than the designed value. The fabricated reflectivity of 95.8% is lower than the designed value 99.8%. Every layer thickness is not easy to control, leading to the real refractive index different from the designed index. Fig.4 shows 30°-inclined top SEM image of the fabricated VCSEL. The circular current confinement diameter is 12 μm. The circular mesa diameter for light window is 56 μm. The top contact ring size is 20 μm. The pad contact area is 100 μm×100 μm.

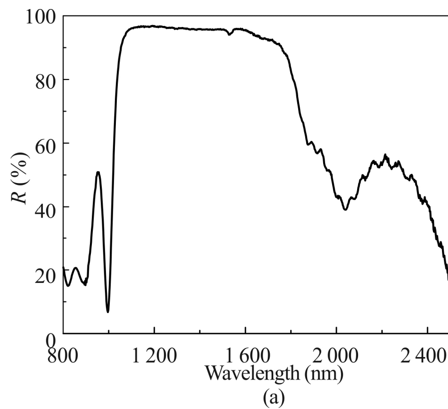


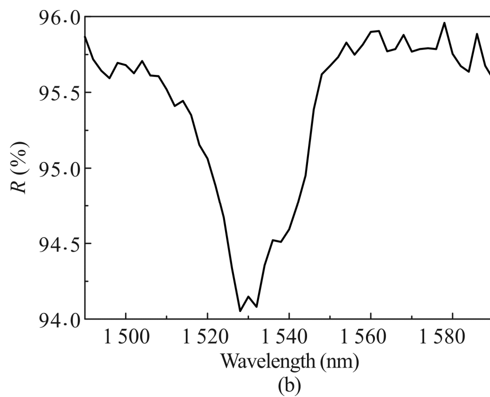


**Fig.3 (a) Reflectivity spectrum of the fabricated VCSEL epitaxial structure; (b) Reflectivity spectrum of the fabricated VCSEL cavity mode**

To capture the whole power, the devices were mounted in a conventional PCB test chip. Fig.5 shows *I-V* characteristics of the fabricated VCSEL under CW operation at room temperature. Fig.6 shows *I-L* characteristics of the fabricated VCSEL under CW operation at room temperature. The threshold current is 40 mA. The power was measured by an optical spectrometer. The maximum output power is around −7.17 dBm from Fig.6. This is because of the carrier leak in the current-light confinement area resulting in quantum efficiency reduction. The reflectivity 95% of epitaxial layers is lower. The solution is improving proton implant and increasing reflectivity of top DBR. Fig.7 shows the electroluminescence spectrum under 60 mA DC current injection. The lasing occurred at 1 526 nm in Fig.7. Compared with Fig.3(b), the lasing wavelength 1 526 nm is shorter than the cavity mode wavelength 1 530 nm. The main reason may be Joule heat. The Joule heat comes from laser itself, dielectric top DBR, PCB test broad. The Joule heat can result in material index variation, absorption and loss increasing. The full width at half maximum (FWHM) of lasing spectrum is about 5 nm. One reason is that carrier leak in the current-light confinement area resulted in quantum efficiency reduction. The other reason is active MQW gain increasing.

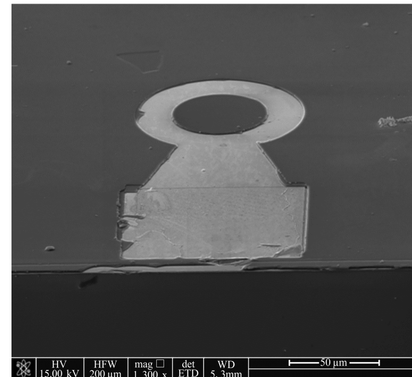


**Fig.4 30° inclined top SEM image of the fabricated VCSEL sample**

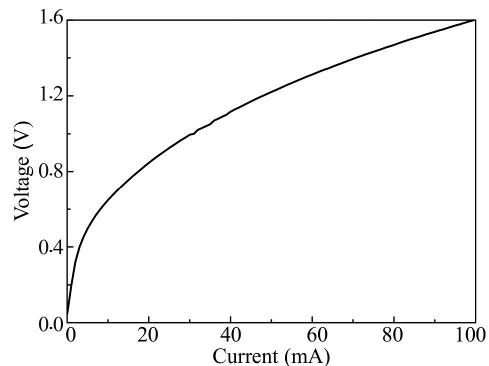


**Fig.5 *I–V* characteristics of the fabricated VCSEL at room temperature**

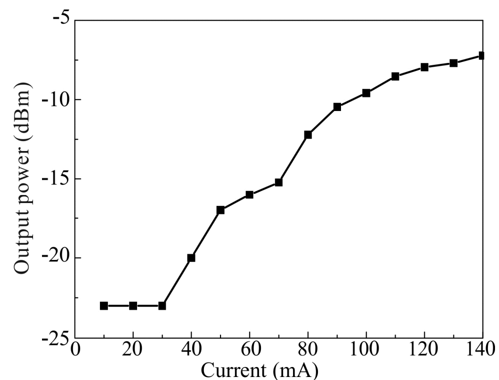


**Fig.6 Plot of *I–L* characteristics of the fabricated VCSEL at room temperature**

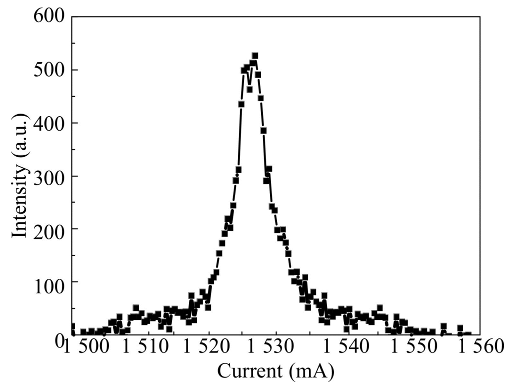


**Fig.7 Lasing spectrum of the VCSEL at an injection current of 60 mA**

In conclusion, a 1 550 nm long-wavelength VCSEL on InP substrate has been designed and fabricated. The designed cavity mode is around 1 536 nm. The dip of fabrication cavity mode is around 1 530 nm. The threshold current is 40 mA under CW operation at room temperature. The lasing occurred at 1 526 nm. The long wavelength VCSELs are promising to be applied in long reach data communication.

## References


[1] M. Xun, Ch. Xu, Y Y. Xie, G Q. Jiang, J. Wang, K. Xu and H D. Chen, Optics Letters **40**, 12349 (2015).

[2] H Y. Qiu, Zh M. Wu, T. Deng, Y. He and G Q. X, Chinese Optics Letters **14**, 021401 (2016).

[3] Su Y M, Yu L J, Guo X, Zhang X, Liu J G and Zhu N H, Journal of Semiconductors **38**, 9 (2017).

[4] M K. Li, L J. Yuan, H Y. Yu, Q. Kan, Sh Y. Li, J P. Mi and J Q. Pan, Journal of Semiconductors **37**, 034007 (2016).

[5] M C Y. Huang, Y. Zhou and C. Chang-Hasnain, Nature Photonics **1**, 119 (2007).

[6] H Y. Kao, C T. Tsai, C Y. Pong, Sh F. Liang, Z K. Weng, Y Ch. Chi, H Ch. Kuo, J J. Huang, T Ch. Lee, Ti T Shih, J J. Jou, W H. Cheng, Ch-H Wu and G R. Lin, Few-Mode 850nm VCSEL Chip with Direct 16-QAM OFDM Encoding at 80-Gbit/s for 100-m OM4 MMF Link, Optical Fiber Communications Conference, Th2A.38 (2017).

[7] H. Soda, K. Iga, C. Kitahara and Y. Suematsu, Japanese Journal of Applied Physics **18**, 2329 (1979).

[8] W. Hofmann, M. Müller, A. Nadtochiy, Ch. Meltzer, A. Mutig, G. Bohm, J. Rosskofk, D. Bimberg, M Ch. Amann and C. Chang-Hasnain, Optics Express **17**, 17547 (2009).

[9] C. Chase, Y. Rao, W. Hofmann and C J. Chang-Hasnain, Optics Express **18**, 15461 (2010).

[10] M C. Amann and W. Hofmann, IEEE Journal of Selected Topics in Quantum Electronics **15**, 861 (2009).

[11] M. Ortsiefer, R. Shau, F. Mederer, R. Michalzik, J. Rosskopf, G. Bohm, F. Kohler, C. Lauer, M. Maute and M.-C. Amann, Electronics Letters **38**, 1180 (2002).

[12] L. Chrostowski, B. Faraji, W. Hofmann, M Ch. Amann, S. Wieczorek and W W. Chow, IEEE Journal of Selected Topics in Quantum Electronics **13**, 1200 (2007).

[13] Y. Huang, X. Zhang and J. Zhang, IEEE Photonics Journal **9**, 4 (2017).

[14] H. Yu, S. Yao and G. Zhou, Optical & Quantum Electronics **50**, 4 (2018).

[15] Y. Feng, P. Liu and D. Feng, High-speed Oxidation-confined 850nm VCSELs, IEEE International Conference on Optoelectronics and Microelectronics, 389 (2016).

[16] T. Fang, B. Cui and S. Hao, Journal of Semiconductors **39**, 2 (2018).

[17] J. Wen, Y M. Wen, P. Li and S Sh. W, Journal of Semiconductors **37**, 064010 (2016).

[18] M. Born and E. Wolf, Principles of Optics, 6th edn, Pergamon Press, Oxford, 1989.

[19] Dan Y, Levi M and Karni Y, Facet Engineering of High Power Single Emitters, Proceedings of SPIE - The International Society for Optical Engineering, 7918 (2011).